Resonance radiation transport in plasma display panels

Resonance radiation transport in plasma display panels

G. J. M. Hagelaar[a)]

Department of Physics, Eindhoven University of Technology, P.O. Box 513, 5600 MB Eindhoven, The Netherlands

M. H. Klein and R. J. M. M. Snijkers

Philips Research Laboratories Aachen, Weisshausstrasse 2, 52066 Aachen, Germany

G. M. W. Kroesen

Department of Physics, Eindhoven University of Technology, P.O. Box 513, 5600 MB Eindhoven, The Netherlands

In fluid models of the gas discharges in plasma display panels, the trapping of resonance radiation is usually accounted for by a trapping factor. In this work, we present a Monte Carlo model for resonance photons, which gives a much more accurate description. First, we compare the results of this Monte Carlo model with the results of the fluid model trapping factor approach. Although the trapping factor approach does not yield the same spatial distribution for the density of the resonant state atoms, the spatially integrated density is in good agreement with the results of the Monte Carlo model. Next, we compare the results of the Monte Carlo model with measured spectra of emitted resonance radiation. The agreement is very good. Thus we provide, via the Monte Carlo model, experimental support for the widely used trapping factor approach. © *2000 American Institute of Physics.* [S0021-8979(00)06723-2]

I. INTRODUCTION

Plasma display panel (PDP) technology is a promising technology for large, lightweight, flat displays.[1] Color PDPs use small high-pressure glow discharges in xenon mixtures to generate ultraviolet (UV) radiation and to convert this into red, blue, and green light by phosphors. In the research and development of PDPs, numerical fluid models are widely used to calculate the yield of UV radiation from PDP discharges. Examples of such calculations can be found in Refs. 2–4.

The most important UV radiation utilized in PDPs is the resonance radiation emitted by the $Xe^*(^3P_1)$ state atoms at a wavelength of 147 nm. The PDP discharge conditions are such that these resonance photons are absorbed and re-emitted many times before leaving the discharge. This phenomenon is known as imprisonment or trapping of resonance radiation. The most obvious effect of the radiation trapping is that the photons emerge from the discharge on a time scale that is much longer than the natural lifetime of the resonant state. Another effect is that the density of the resonant state atoms is enormously increased. This affects the entire kinetics of the excited species in the discharge, because the rates of several important reactions, including collisional quenching of the resonant state and the formation of dimers, depend on the density of these atoms. As an illustration, Table I gives an overview of the most important reactions involving $Xe^*(^3P_1)$ in PDP discharges in neon–xenon; the time dependent rates of some of these reactions are shown in Fig. 1. To properly predict the production of UV radiation in PDP

discharges, fluid models have to account for the effects of radiation trapping.

The exact calculation of the density of the resonant state atoms under the influence of radiation trapping requires the solution of an integro differential equation, such as Holstein's equation.[5] However, solving such an equation in time dependent fluid models is in practice not feasible. Most fluid models[2,6,7] describe the resonant state by an ordinary differential equation, a rate equation or a continuity equation, in which they characterize the radiative decay by an effective lifetime

$$\tau_{\text{eff}} = g\,\tau_0, \tag{1}$$

rather than by the natural lifetime τ_0. Here g is a trapping factor, which represents the average number of absorption-reemission events that a resonance photon undergoes before escaping from the discharge. (Some authors use g^{-1} to indicate what we call g.) The trapping factor is usually derived from a known solution of Holstein's equation for some symmetric geometry. Standard expressions for trapping factors under various assumptions can be found in Refs. 8 and 9. The trapping factor approach simulates, in a computationally very attractive way, the major effects of radiation trapping: it slows down the release of resonance photons and increases the density of the resonant state atoms. It does, however, not describe the spatial evolution of the resonant state density.

An alternative and more accurate way to describe the radiation trapping is by a Monte Carlo model for resonance photons. Besides the density of the resonant state atoms, a photon Monte Carlo model predicts the spectral line shape of the resonance radiation escaping from the discharge. This offers the possibility of direct experimental validation of the

---
[a)]Electronic mail: hagelaar@discharge.phys.tue.nl

TABLE I. Most important reactions involving $Xe^*(^3P_1)$ in typical PDP discharges in neon–xenon.

No.	Reaction
	Production
R1	$e + Xe \rightarrow e + Xe^*(^3P_1)$
R2	$Xe^{**} + Ne \rightarrow Xe^*(^3P_1) + Ne$
R3	$Xe^{**} + Xe \rightarrow Xe^*(^3P_1) + Xe$
R4	$Xe^{**} \rightarrow Xe^*(^3P_1) + h\nu(800\ nm)$
	Loss
R5	$e + Xe^*(^3P_1) \rightarrow e + Xe^{**}$
R6	$Xe^*(^3P_1) + Ne \rightarrow Xe^*(^3P_2) + Ne$
R7	$Xe^*(^3P_1) + Xe + Ne \rightarrow Xe_2^*(O_u^+) + Ne$
R8	$Xe^*(^3P_1) + 2Xe \rightarrow Xe_2^*(O_u^+) + Xe$
R9	$Xe^*(^3P_1) \rightarrow Xe + h\nu(147\ nm)$

model. In this article we present such a Monte Carlo model of the resonance photons in PDPs. The photon Monte Carlo model requires the input of the rates of collision processes that lead to the formation of the resonant state. For this we use the results of the fluid model presented in Ref. 10. For reasons of simplicity, the Monte Carlo model is not self-consistently coupled to the fluid model; it just uses reaction rates that have been calculated *a priori* with the fluid model. This approach is legitimate because the rates concerned are only weakly coupled to the radiation trapping problem. In the fluid model, the radiation trapping is accounted for with the trapping factor approach (Eq. (1)).

In this article, we do the following: After describing the Monte Carlo model in Sec. II, we compare, in Sec. III, the calculated resonant state atom density profile with the density profile resulting from the trapping factor approach in the fluid model. Then, in Sec. IV, we compare the calculated emission spectrum with experimental data. The conclusions are given in Sec. V. All calculations presented are based on the two-dimensional model geometry shown in Fig. 2, which represents a cross section through one row of a coplanar-electrode PDP. The discharge conditions considered are also
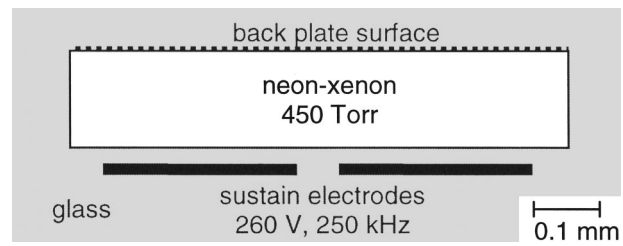
FIG. 2. Two-dimensional model geometry considered in the calculations, representing one discharge cell of a coplanar-electrode type PDP. The surface on the top corresponds to the back plate of the display, where the phosphors are located.

indicated in Fig. 2: The discharge gas is a mixture of neon and a small percentage of xenon, at a pressure of 450 Torr, and the square wave voltage applied to the sustain electrodes has an amplitude of 260 V and frequency of 250 kHz.

II. PHOTON MONTE CARLO MODEL

In the Monte Carlo model, a large number of resonant state excitation events is sampled from the total excitation rate profile calculated with the fluid model. The resonance photons that result from these excitation events, are followed, one by one, until they escape from the discharge. Since the escape time of the photons is much longer than the typical time scale for changes in the excitation rate, the Monte Carlo model is not suitable to study the time dependence of the radiation transport. We can, however, still calculate the time averaged photon transport. Below we describe how a photon path is simulated.

We start from the time averaged effective excitation rate profile, shown in Fig. 3. It is the sum of the rates of the reactions R1, R2, R3, and R4, diminished with the rate of reaction R5. An excitation event is randomly sampled from this profile. A random lifetime τ of the resulting resonant state is determined, according to

$$\tau = -\frac{1}{\nu}\ln(1 - r_1), \tag{2}$$

where r_1 is a random number, uniformly distributed between 0 and 1, generated with a random number computer routine, and ν is given by

$$\nu = \frac{1}{\tau_0} + \nu_c. \tag{3}$$

Here $\tau_0 = 3.46\ ns$ is the natural lifetime[11] of $Xe^*(^3P_1)$ and ν_c is the total frequency of the collision processes R6, R7,
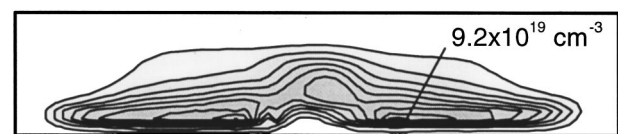
FIG. 3. Time averaged profile of the effective excitation rate of $Xe^*(^3P_1)$ calculated with the fluid model. The discharge geometry and conditions are shown in Fig. 2; the xenon percentage is 5%. The averaging was done over one address pulse and five sustain pulses. The increment of the contours is $9.2 \times 10^{18}\ cm^{-3}$.
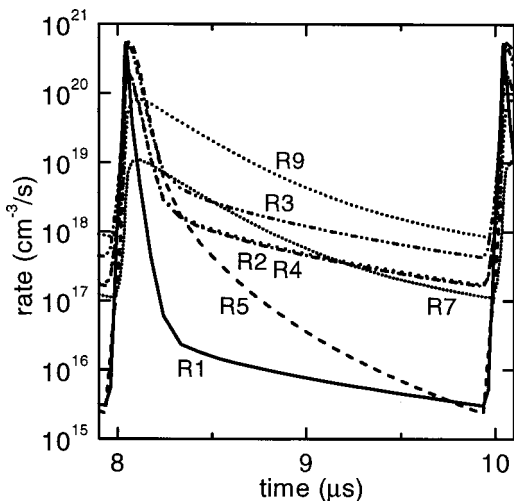

FIG. 1. Time evolution of the space averaged reaction rates of the most important processes involving the $Xe^*(^3P_1)$ state in a fluid simulation of a typical PDP discharge in neon–xenon (5%). The curves are tagged with the numbers of the corresponding reactions in Table I. The time interval from 8 to 10 μs corresponds to one sustain pulse.

R8, and R9. Note that ν_c is constant in time. The time dependent frequency of electron induced quenching R5 is not included in ν_c; this reaction is taken into account in the effective excitation rate profile. (Fig. 1) This crude treatment of the electron induced quenching is somewhat justified by the fact that this process, like the excitation, takes place only during a short fraction of the time, as can be seen in Fig. 1. Another random number r_2 is used to determine whether a photon is emitted or the resonant state is lost in a collision process; if $r_2 > \tau \nu_c$ the photon is emitted, otherwise the resonant state is lost.

In the event that a photon is emitted, a random photon frequency is chosen. We assume that the frequency distribution is mainly determined by the broadening of the $Xe^*(^3P_1)$ level due to collisions between the gas atoms, and is given by the Lorentz profile,

$$L(\omega) = \frac{\Delta\omega_p/(2\pi)}{(\omega-\omega_0)^2 + \Delta\omega_p^2/4}, \tag{4}$$

where ω is the angular frequency, ω_0 is the central angular frequency (1.28×10^{16} Hz), and $\Delta\omega_p$ is the full width at half maximum. For the width of the profile we use the experimental data from Ref. 12:

$$\Delta\omega_p = 2.55 \times 10^{-14} n_{Xe} + 1.00 \times 10^{-15} n_{Ne}, \tag{5}$$

where n_{Xe} and n_{Ne} are the xenon and neon densities in m^{-3}. The influence of the Doppler effect on the frequency distribution is neglected compared to the collisional broadening (4), which seems a good approximation for partial xenon pressures beyond 10 Torr. A random angular frequency ω is chosen from the distribution, Eq. (4), as

$$\omega = \omega_0 + \frac{\Delta\omega_p}{2}\tan\left(\frac{\pi}{2}(2r_3-1)\right), \tag{6}$$

where r_3 is a random number.

Given the photon frequency, the absorption coefficient is calculated from

$$\kappa(\omega) = \frac{\lambda_0^2 g_2}{4\tau_0 g_1} n_{Xe} L(\omega), \tag{7}$$

where $L(\omega)$ is once again the Lorentz profile, (4), $\lambda_0 = 147$ nm is the central wavelength, and $g_1 = 1$ and $g_2 = 3$ are the statistical weights of the ground and resonant states, respectively. A random value for the traveled distance until absorption is found as

$$\lambda = -\frac{1}{\kappa}\ln(1-r_4), \tag{8}$$

in analogy to Eq. (2). Using two additional random numbers, r_5 and r_6, a random direction is determined for photon emission, after which the position of the absorption is calculated. The lifetime of the resulting resonant state is again determined from Eq. (2), and so on. The procedure is repeated until the photon reaches the wall or the resonant state is lost in a collision. Note that, each time the photon is re-emitted, we assume that its frequency is independent of the frequency before absorption. This condition is known as complete frequency redistribution.
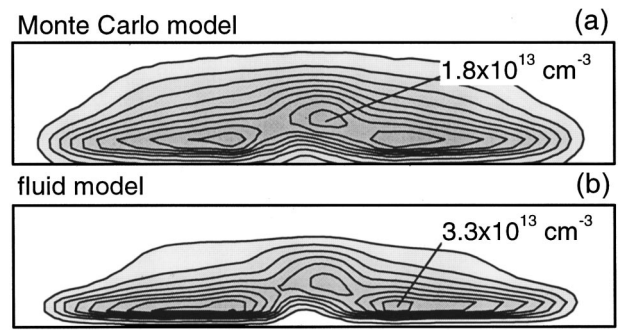

FIG. 4. Calculated spatial profile of the resonant state atom density for (a) the Monte Carlo model and (b) the fluid model using a trapping factor of $g = 155$. The discharge geometry and conditions are shown in Fig. 2; the xenon percentage is 5%. The increment of the contours is 1/10 times the maximum value.

For storage of Monte Carlo calculation results, the geometry is divided into small two-dimensional cells. We make use of the numerical grid of the fluid model. In each grid cell we record the cumulative lifetime of the resonant state. From this, the resonant state atom density can be directly derived. In a similar way, the photon frequency distribution is determined in every cell by recording the cumulative time of photon presence separately for a large number of frequency intervals.

III. COMPARISON WITH THE TRAPPING FACTOR APPROACH

We simulated the paths of 10^7 photons, initially emitted according to the effective excitation rate profile of Fig. 3. Figure 4(a) shows the calculated spatial density profile of the resonant state atoms. For comparison, Fig. 4(b) shows the resonant state density that results from the trapping factor approach in the fluid model. According to the Monte Carlo model, the resonant state atoms are much more distributed over space than they are in the fluid model. This result is not surprising: with the trapping factor approach, the resonant states created are not spatially redistributed, so their density profile directly reflects the effective excitation profile of Fig. 3. The spatial integral of the density (the total number of resonant state atoms per cm of row length) is approximately the same for both models: in the Monte Carlo model it is 4.9×10^9 cm^{-1}, compared to 5.1×10^9 cm^{-1} for the fluid model.

One has to keep in mind that the density in the fluid model depends directly on the choice for the trapping factor g. Typically, g is estimated from the solution of Holstein's equation for a plane-parallel slab geometry:[5,8]
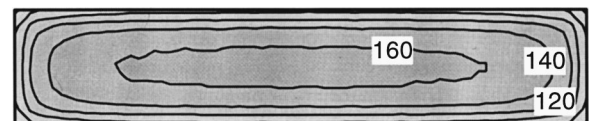

FIG. 5. Spatial profile of the average escape time for the geometry in Fig. 2; the gas pressure is 450 Torr, and the xenon percentage is 5%. The values indicated are expressed in units of $\tau_0 = 3.46$ ns. The increment of the contours is $20\tau_0$.
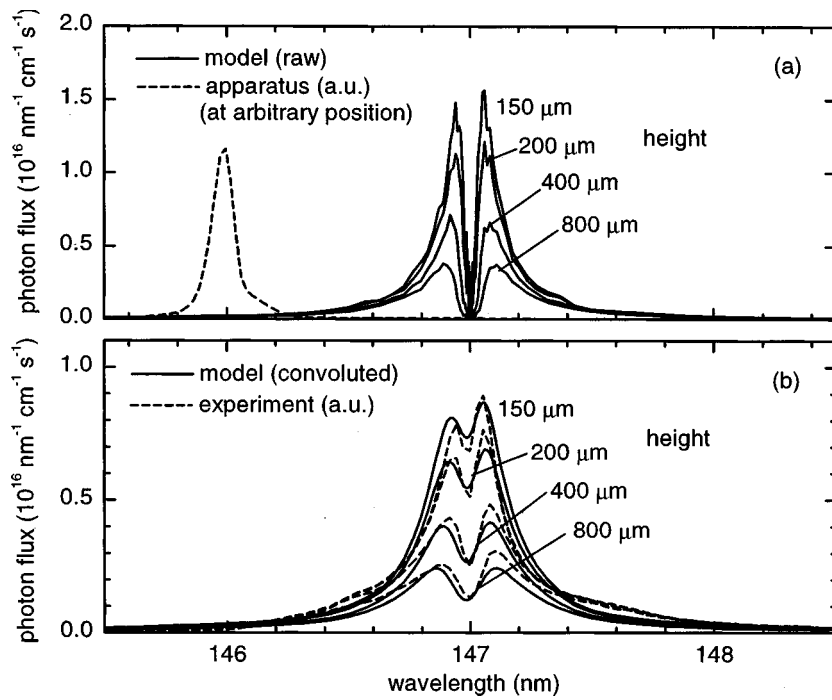
FIG. 6. Spectrum of the resonance photons leaving the discharge at the back plate for different cell heights. Each time the geometry and conditions are similar to the model geometry and conditions shown in Fig. 2; the xenon percentage is 10%. (a) Results of the Monte Carlo model, as well as the experimental apparatus profile. (b) Comparison of the convoluted modeling results and the experimental results.

$$g = \frac{1}{1.146} \sqrt{\pi \kappa_0 d}, \tag{9}$$

where κ_0 is the absorption coefficient for the central frequency and d is the thickness of the slab. Equation (9) is based on the same assumptions as the ones we make in the Monte Carlo model, and the additional assumption that $\kappa_0 d \gg 1$. On substituting $d = 1.50 \times 10^{-4}$ m, the height of the model geometry, and $\kappa_0 = 6.70 \times 10^7$ m^{-1}, calculated from Eqs. (4), (5), and (7), we find $g = 155$. It is interesting to compare this trapping factor to the escape time of the photons in the Monte Carlo model. To obtain a proper comparison, we set the collisional loss frequency of the resonant

state to zero, and again simulated 10^7 photon paths. Figure 5 shows for each position in the model geometry the average escape time of photons initially emitted from that position. As can already be expected from Eq. (9), the escape time changes only weakly over space. The average escape time of the photons initially emitted according to the excitation rate profile of Fig. 3 turns out to be 150 τ_0, in good agreement with the trapping factor $g = 155$.

IV. COMPARISON WITH EXPERIMENTAL RESULTS

Due to the radiation trapping, the spectral line shape of the resonance radiation that leaves the discharge is very different
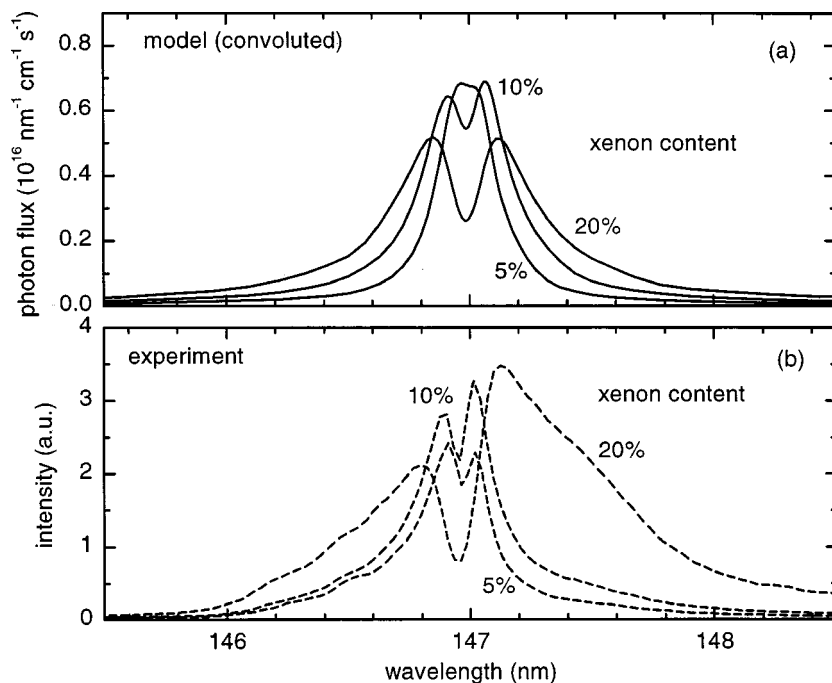

FIG. 7. Spectrum of resonance photons leaving the discharge at the back plate for different percentages of xenon. Each time the geometry and conditions are similar to the model geometry and conditions shown in Fig. 2; the cell height is 150 μm. Comparison of (a) the results of the Monte Carlo model after convolution with the experimental apparatus profile and (b) the measured spectra.

from the emitted Lorentz profile (4). This can be seen as follows: Every time a photon is absorbed, it has a small probability of being re-emitted in the wings of the Lorentz distribution, where it has a good chance of escaping from the discharge without being absorbed again. Accordingly, the frequency distribution of the escaping photons has stronger wings than the Lorentz profile, and consequently a weaker center. Under PDP conditions, the line shape becomes broader by orders of magnitude, and even displays a minimum at the central frequency. Figure 6(a) shows the spectrum of the resonance photons that leave the discharge at the back plate, calculated with the Monte Carlo model, for different cell heights; these results are obtained by integration over the back plate surface indicated in Fig. 3. Note that here the actual width of the Lorentz profile is no more than 3.7×10^{-3} nm.

In order to check the validity of the model, we measured the emitted spectrum. The measurement setup is similar to the one used in Ref. 13. The photons enter a vacuum UV monochromator (Acton Research VM 504) through a MgF_2 observation window placed at the position of the back plate. Spectral information is read out via an intensified charge coupled device camera (Princeton Instruments, IVUV 576 $\times$384 E) and is spectrally corrected. The experimental discharge geometry is very similar to that of the model geometry of Fig. 3; the most important difference is that the experimental geometry has additional side walls, which confine the discharge in the direction of the sustain electrodes and represent the barrier ribs of a real display.

In order to be able to directly compare the calculated spectrum with the measurements, we convolute it with the experimental apparatus profile. This profile, which we assume to be identical to the measured profile of the 436 nm mercury line, is shown in Fig. 6(a). The convoluted calculated spectrum is compared with the measured spectrum in Fig. 6(b) for different cell heights, and in Fig. 7 for different percentages of xenon. The overall agreement is very good: The width of the line shape, the width of the central dip, and even the relative intensities for the different conditions are predicted well by the model. However, there are some differences: After convolution, the central dip in the calculated spectrum is less pronounced than the dip in the experimental spectrum. This suggests that the assumed apparatus profile is slightly wider than the actual apparatus profile. In addition, the wings of the measured line shape are sometimes stronger than they are in the calculation, especially at higher xenon

pressures. For 20% xenon, the measured spectrum is also strongly asymmetric, as can be seen in Fig. 7(b). These effects could well be caused by the molecular radiation emitted by higher vibrational levels of $Xe_2^*(O_u^+)$.

V. CONCLUSIONS

We have presented a Monte Carlo model for the transport of resonance radiation in PDPs. First, we have compared the results of this Monte Carlo model with the results of the commonly used trapping factor approach. Although the trapping factor approach does not yield the same spatial distribution for the density of the resonant state atoms, the spatially integrated density is in good agreement with the results of the Monte Carlo model. Next, we have compared the results of the Monte Carlo model with measured spectra of resonance radiation. The agreement is very good. The minor differences between model and experiment can be easily be attributed to experimental artifacts and do not give rise to doubts about the assumptions of the model.

The overall conclusion is that, via the Monte Carlo model, we have provided experimental support for the widely used trapping factor approach.

ACKNOWLEDGMENT

[1] L. Weber, in *Flat-Panel Displays and CRTs*, edited by L. Tannas (Van Nostrand Reinhold, New York, 1985), pp. 332–407.
[2] J. Meunier, Ph. Belenguer, and J. P. Boeuf, J. Appl. Phys. **78**, 731 (1995).
[3] S. Rauf and M. J. Kushner, J. Appl. Phys. **85**, 3470 (1999).
[4] G. J. M. Hagelaar, M. H. Klein, R. J. M. M. Snijkers, and G. M. W. Kroesen, J. Appl. Phys. (submitted).
[5] T. Holstein, Phys. Rev. **83**, 1159 (1951).
[6] R. T. McGrath, R. Veerasingam, J. A. Hunter, P. D. Rockett, and R. B. Campbell, IEEE Trans. Plasma Sci. **26**, 1532 (1998).
[7] S. Rauf and M. J. Kushner, J. Appl. Phys. **85**, 3460 (1999).
[8] A. F. Molisch, B. P. Oehry, and G. Magerl, J. Quant. Spectrosc. Radiat. Transf. **48**, 377 (1992).
[9] A. F. Molisch, B. P. Oehry, W. Schupita, and G. Magerl, J. Quant. Spectrosc. Radiat. Transf. **49**, 361 (1993).
[10] G. J. M. Hagelaar, G. M. W. Kroesen, U. van Slooten, and H. Schreuders, J. Appl. Phys. **88**, 2252 (2000).
[11] J. Berkowitz, *Photoabsorption, Photoionization, and Photoelectron Spectroscopy* (Academic, London, 1979).
[12] K. Igarashi, S. Mikoshiba, Y. Watanabe, M. Suzuki, and S. Murayama, J. Phys. D **28**, 1377 (1985).
[13] H. Jeong, J. Seo, C. Yoon, J. Kim, and K.-W. Whang, J. Appl. Phys. **85**, 3092 (1999).